

## Proton Magnetic Shielding Tensor in Liquid Water

Kristofer Modig and Bertil Halle\*

Contribution from the Department of Biophysical Chemistry, Lund University,  
Box 124, SE-22100 Lund, Sweden

Received May 21, 2002

**Abstract:** The nuclear magnetic shielding tensor is a sensitive probe of the local electronic environment, providing information about molecular structure and intermolecular interactions. The magnetic shielding tensor of the water proton has been determined in hexagonal ice, but in liquid water, where the tensor is isotropically averaged by rapid molecular tumbling, only the trace of the tensor has been measured. We report here the first determination of the proton shielding anisotropy in liquid water, which, when combined with chemical shift data, yields the principal shielding components parallel ( $\sigma_{\parallel}$ ) and perpendicular ( $\sigma_{\perp}$ ) to the O–H bond. We obtained the shielding anisotropy  $\sigma_{\parallel} - \sigma_{\perp}$  by measuring the proton spin relaxation rate as a function of magnetic induction field in a water sample where dipole–dipole couplings are suppressed by H/D isotope dilution. The temperature dependence of the shielding components, determined from 0 to 80 °C, reflects vibrational averaging over a distribution of instantaneous hydrogen-bond geometries in the liquid and thus contains unique information about the temperature-dependent structure of liquid water. The temperature dependence of the shielding anisotropy is found to be 4 times stronger than that of the isotropic shielding. We analyze the liquid water shielding components in the light of previous NMR and theoretical results for vapor and ice. We show that a simple two-state model of water structure fails to give a consistent interpretation of the shielding data and we argue that a more detailed analysis is needed that quantitatively relates the shielding components to hydrogen bond geometry.

### 1. Introduction

When a uniform magnetic field is applied to a molecular system, electronic currents are induced that create secondary magnetic fields. This effect, described by the magnetic shielding tensor  $\sigma$ , can be studied via the Zeeman interaction of nuclear magnetic moments.<sup>1</sup> The magnetic nucleus thus becomes a sensitive probe of the local electron distribution, providing information about molecular structure. Moreover, the shielding tensor is affected when a molecule is brought from an ideal gas into a condensed phase. This intermolecular contribution to the shielding tensor is due to induced electronic currents in nearby molecules and to the perturbing effect of intermolecular interactions on the electron distribution and nuclear geometry of the reference molecule. The shielding tensor can thus be used as a probe of intermolecular structure and interactions in liquids and solids.

In liquids, the shielding tensor is orientationally averaged by molecular tumbling and the NMR frequency only provides information about the isotropic average,  $\sigma_{\text{iso}} = \text{Tr } \sigma/3$ . This isotropic shielding gives rise to the chemical shift that endows NMR spectroscopy with atomic resolution and, additionally, provides information about intermolecular interactions. For example, the “downfield” shift of the <sup>1</sup>H resonance caused by proton deshielding (reduced  $\sigma_{\text{iso}}$ ) is routinely used as a qualitative indicator of hydrogen bonding.<sup>2,3</sup> In solids, all three principal components of (the symmetric part of) the shielding

tensor, as well as its orientation, can be determined with line narrowing techniques.<sup>4</sup> In particular, one can obtain the shielding anisotropy,  $\Delta\sigma = \sigma_{\parallel} - \sigma_{\perp}$ , which is even more sensitive to hydrogen bonding than  $\sigma_{\text{iso}}$ .<sup>5</sup> From such solid-state NMR experiments, combined with neutron diffraction data, correlations between shielding tensor components and hydrogen bond geometry have been established.<sup>6,7</sup>

As a result of recent advances in ab initio computational methodology, it is now possible to relate the shielding tensor to hydrogen-bond geometry in a quantitative way even for condensed phases.<sup>8–12</sup> To fully capitalize on these theoretical advances, one would like to experimentally determine the shielding anisotropy in liquids. This can be accomplished by measurements of spin relaxation rates, which, through their second-order dependence on the spin Hamiltonian, contain information about the anisotropy of the shielding tensor.<sup>1</sup> The utility of this approach is limited, especially for protons, by the fact that the shielding anisotropy (SA) interaction usually is

- (2) Becker, E. D. In *Encyclopedia of Nuclear Magnetic Resonance*; Grant, D. M., Harris, R. K., Eds.; Wiley: Chichester, 1996; pp 2409–2415.
- (3) Konrat, R.; Tollinger, M.; Kontaxis, G.; Kräutler, B. *Monatsh. Chem.* **1999**, *130*, 961–982.
- (4) Brunner, E.; Sternberg, U. *Prog. NMR Spectrosc.* **1998**, *32*, 21–57.
- (5) Ditchfield, R. *J. Chem. Phys.* **1976**, *65*, 3123–3133.
- (6) Berglund, B.; Vaughan, R. W. *J. Chem. Phys.* **1980**, *73*, 2037–2043.
- (7) Wu, G.; Freure, C. J.; Verdurand, E. *J. Am. Chem. Soc.* **1998**, *120*, 13 187–13 193.
- (8) de Dios, A. C. *Prog. NMR Spectrosc.* **1996**, *29*, 229–278.
- (9) Helgaker, T.; Jaszunski, M.; Ruud, K. *Chem. Rev.* **1999**, *99*, 293–352.
- (10) Malkin, V. G.; Malkina, O. L.; Steinebrunner, G.; Huber, H. *Chem. Eur. J.* **1996**, *2*, 452–457.
- (11) Mauri, F.; Pfrommer, B. G.; Louie, S. G. *Phys. Rev. Lett.* **1996**, *77*, 5300–5303.
- (12) Sebastiani, D.; Parrinello, M. *J. Phys. Chem. A* **2001**, *105*, 1951–1958.

\* Address correspondence to this author. E-mail: bertil.halle@bpc.lu.se.

(1) Abragam, A. *The Principles of Nuclear Magnetism*; Clarendon Press: Oxford, 1961.

much weaker than other anisotropic nuclear spin couplings. Under normal conditions,  $^1\text{H}$  spin relaxation is therefore strongly dominated by the nuclear magnetic dipole–dipole (DD) coupling. This problem can be overcome in two ways. One approach exploits temporal cross-correlation between the SA and DD couplings, which opens up new relaxation pathways in coupled spin systems.<sup>13</sup> In recent years, such relaxation interference effects have been studied extensively for heavier nuclides, such as  $^{13}\text{C}$  and  $^{15}\text{N}$ .<sup>14</sup> The other approach, which is the one adopted here, is isotope dilution, whereby the dominant DD coupling is suppressed by substitution with an isotope with small (or no) magnetic moment.

The unique physical properties of liquid water can be traced to the ability of water molecules to form transient three-dimensional networks of hydrogen bonds.<sup>15–17</sup> Accordingly, most attempts at modeling the structure of liquid water and its dependence on temperature, pressure, and solute perturbations have focused on the geometry, energetics, and connectivity of hydrogen bonds. Experimental information about hydrogen bonding in liquid water has come mainly from vibrational spectroscopy and, indirectly, from X-ray and neutron diffraction. Although NMR has contributed greatly to our understanding of molecular dynamics in water, it has taught us little about the structure of liquid water. Attempts have been made to extract structural information from the temperature-dependent isotropic shielding  $\sigma_{\text{iso}}$  in water.<sup>18–24</sup> These attempts were inconclusive for two reasons. First, the two parameters (a distance and an angle) needed to define the (average) hydrogen-bond geometry cannot be deduced from a single observable ( $\sigma_{\text{iso}}$ ). Second, the quantum-mechanical calculations required to quantitatively relate the shielding tensor to the intermolecular geometry of water have only recently been carried out.<sup>25</sup> The present work was motivated by these calculations and by the realization that the shielding anisotropy can be experimentally determined, thereby removing the ambiguity in interpretation.

Proton spin relaxation in liquid water has been thoroughly studied since the early days of NMR.<sup>26</sup> In the absence of paramagnetic impurities, the longitudinal relaxation time,  $T_1 = 3.6$  s for  $\text{H}_2\text{O}$  at 25 °C,<sup>27</sup> is heavily dominated by DD couplings between intra- and intermolecular proton pairs. At high temperatures, there is also a small contribution from coupling of the nuclear magnetic moment with the magnetic field generated by the rotating molecular charge distribution (spin–rotation coupling). There should also be a small contribution from the proton shielding anisotropy, which appears to have escaped

detection in all previous studies. This is not surprising, for even in the highest NMR field in common use today (18.8 T) the SA contribution is merely a few percent of the DD contribution. As demonstrated here, however, the SA contribution can be accurately measured if the DD contribution is suppressed by isotopic dilution; one simply measures the proton relaxation of HDO in  $\text{D}_2\text{O}$  doped with a small amount of  $\text{H}_2\text{O}$ .<sup>28,29</sup> In this way, the SA contribution can be enhanced to about 25% at 18.8 T.

We report here the results of relaxation measurements over the field range 2.35–18.8 T on a sample of  $\text{D}_2\text{O}$  containing 1%  $\text{H}_2\text{O}$  and studied at nine temperatures in the range 0–80 °C. The quadratic field dependence allows us to isolate the SA contribution to the relaxation rate and to obtain, at each temperature, the product of  $\langle\Delta\sigma\rangle_V$  and a correlation time defined as the integral of a, possibly complicated, orientational time correlation function. The only water rotational correlation time that has been rigorously determined is that associated with the  $^1\text{H}$ – $^{17}\text{O}$  DD coupling.<sup>30–32</sup> Because the shielding tensor has virtually the same orientation and symmetry as this DD coupling tensor, the two relaxation mechanisms involve the same orientational time correlation function. This fortunate circumstance allows us to use the  $^1\text{H}$ – $^{17}\text{O}$  correlation time to deduce the vibrationally averaged shielding anisotropy  $\langle\Delta\sigma\rangle_V$  from our data.

The outline of this paper is as follows. In section 3, we recapitulate the relevant properties of the shielding tensor, and in section 4, we discuss the relaxation mechanisms that could conceivably contribute to the measured relaxation rate. Because  $T_1$  is very long (up to 2 min), we must consider minor relaxation mechanisms that are normally neglected and assess their potential for interfering with the determination of  $\langle\Delta\sigma\rangle_V$ . In section 5 we consider the time correlation function for the fluctuating shielding anisotropy, with particular attention to the effects of vibrational averaging. In section 6, we use literature data on the  $^{17}\text{O}$ -induced  $^1\text{H}$  relaxation in  $\text{H}_2\text{O}$  to obtain the rotational correlation time for the O–H bond that also governs SA relaxation. Then, in section 7, we determine the temperature dependent  $\langle\Delta\sigma\rangle_V$  from our relaxation data with the aid of the results established in the previous sections. Combining our  $\langle\Delta\sigma\rangle_V$  results with  $\langle\sigma_{\text{iso}}\rangle_V$  values obtained from published chemical shifts converted to the absolute shielding scale, we also deduce the shielding tensor components,  $\langle\sigma_{\parallel}\rangle_V$  and  $\langle\sigma_{\perp}\rangle_V$ , parallel and perpendicular to the O–H bond. Finally, in section 8, we compare the shielding tensor components in liquid water with experimental and theoretical results for ice and vapor. We also briefly indicate how the new shielding data can be used to elucidate the temperature-dependent structure of liquid water, a problem that will be more fully addressed in a separate publication.<sup>33</sup>

## 2. Experimental Section

$\text{D}_2\text{O}$  with 99.9 atom % D and low paramagnetic content (Cambridge Isotope Laboratories) was doped with locally purified  $\text{H}_2\text{O}$  (Milli-Q

- (13) Shimizu, H. *J. Chem. Phys.* **1964**, *40*, 3357–3364.
- (14) Kumar, A.; Grace, R. C. R.; Madhu, P. K. *Prog. NMR Spectrosc.* **2000**, *37*, 191–319.
- (15) Eisenberg, D.; Kauzmann, W. *The Structure and Properties of Water*; Clarendon Press: Oxford, 1969.
- (16) Stillinger, F. H. *Science* **1980**, *209*, 451–457.
- (17) Teixeira, J. *J. Physique IV, Coll. C1* **1993**, *3*, 163–169.
- (18) Schneider, W. G.; Bernstein, H. J.; Pople, J. A. *J. Chem. Phys.* **1958**, *28*, 601–607.
- (19) Muller, N.; Reiter, R. C. *J. Chem. Phys.* **1965**, *42*, 3265–3269.
- (20) Muller, N. *J. Chem. Phys.* **1965**, *43*, 2555–2556.
- (21) Hindman, J. C. *J. Chem. Phys.* **1966**, *44*, 4582–4592.
- (22) Rüterjans, H. H.; Scheraga, H. A. *J. Chem. Phys.* **1966**, *45*, 3296–3298.
- (23) Svishchev, I. M.; Goncharov, V. V. *Zh. Strukt. Khim.* **1990**, *31*, 66–70.
- (24) Svishchev, I. M.; Kusalik, P. G. *J. Am. Chem. Soc.* **1993**, *115*, 8270–8274.
- (25) Pfrommer, B. G.; Mauri, F.; Louie, S. G. *J. Am. Chem. Soc.* **2000**, *122*, 123–129.
- (26) Bloembergen, N.; Purcell, E. M.; Pound, R. V. *Phys. Rev.* **1948**, *73*, 679–712.
- (27) Hindman, J. C.; Svirnickas, A.; Wood, M. J. *J. Chem. Phys.* **1973**, *59*, 1517–1522.

- (28) Anderson, W. A.; Arnold, J. T. *Phys. Rev.* **1956**, *101*, 511–512.
- (29) Smith, D. W. G.; Powles, J. G. *Mol. Phys.* **1966**, *10*, 451–463.
- (30) Lankhorst, D.; Schriever, J.; Leyte, J. C. *Ber. Bunsen-Ges. Phys. Chem.* **1982**, *86*, 215–221.
- (31) Struis, R. P. W. J.; de Bleijser, J.; Leyte, J. C. *J. Phys. Chem.* **1987**, *91*, 1639–1645.
- (32) Ludwig, R.; Weinhold, F.; Farrar, T. C. *J. Chem. Phys.* **1995**, *103*, 6941–6950.
- (33) Modig, K.; Pfrommer, B. G.; Halle, B., submitted for publication.

Gradient, Millipore Corp.) to make a water sample with proton fraction  $x_{\text{H}} = 0.0098$ . The sample was contained in a 5 mm o.d. quartz tube (Wilmod Glass Co.), shaped into a cylindrical ampule connected to the upper part of the tube via a narrow constriction. Prior to use, the tube was rinsed with 1% HF, soaked with EDTA solution for 24 h, rinsed repeatedly with deionized water, and finally dried in a vacuum. Dissolved oxygen was removed by several freeze–pump–thaw cycles, whereupon the constriction was flame-sealed under vacuum.

The proton longitudinal relaxation time  $T_1$  was measured at five magnetic field strengths: 2.35, 4.70, 11.75, 14.09, and 18.79 T, using Bruker DMX 100 and 200, General Electrics 500, and Varian INOVA 600 and 800 NMR spectrometers. Measurements were taken at nine temperatures: 0, 4, 15, 27, 40, 50, 60, 70, and 80 °C, recorded with the same calibrated copper–constantan thermocouple (and an ice bath reference) on all spectrometers. The thermocouple was placed in a standard 5 mm NMR tube containing water. This procedure typically yields a precision of 0.1 °C. The temperature drift during the unusually long (2–10 h)  $T_1$  experiments was ca. 0.1 deg below 40 °C, and 0.1–0.5 deg at higher temperatures.

The longitudinal relaxation time  $T_1$  was measured with a saturation recovery pulse sequence, consisting of a saturating aperiodic pulse train of 14 90° pulses with geometrically decreasing spacings (from 4096 to 1 ms), followed by a variable relaxation delay and a 90° detection pulse.<sup>34</sup> This sequence is tolerant to  $B_0$  and  $B_1$  inhomogeneities and to pulse length deviations and it reduces the experiment time considerably, since no equilibration delay is needed between consecutive acquisitions. Within experimental accuracy, the saturation recovery method gave the same  $T_1$  as the traditional inversion recovery method. All measurements were performed with eight cycles and 20 relaxation delays in random order. (Random ordering of delay times is useful for diagnosing temperature fluctuations during the measurement time and for reducing their effect.) The peak area versus delay time was fitted to a three-parameter exponential recovery function by using standard spectrometer software. The standard deviation in the fitted  $T_1$  was usually <0.1% and always <1%. No indications of multiexponential relaxation were seen. Reported relaxation times are averages of up to seven separate measurements. The measured relaxation times ranged from 17 s (0 °C, 18.8 T) to 118 s (80 °C, 2.35 T). The overall experimental uncertainty, taking into account the standard deviation in the fitted  $T_1$ , the effect of the small temperature drift, and the standard deviation of repeated measurements, was usually less than 1% (range 0.2–2.2%). All fits were performed by an in-house implemented version of the Levenberg–Marquardt nonlinear  $\chi^2$  minimizing algorithm.<sup>35</sup>

The measured relaxation rates  $R_1(T, B_0) = 1/T_1(T, B_0)$  constitute a 9 x 5 matrix. The SA contribution could be isolated by separately plotting each matrix row versus  $B_0^2$ . We would then not use our knowledge about the functional form of the temperature dependence. Our analysis of the data suggests that the main source of data scatter is a small temperature error. To suppress this small error, we implemented a smoothing protocol, where the three parameters in the expression  $R_1(T) = aR_1^{\text{DD}}(T) + bR_1^{\text{SR}}(T) + c$  were fitted to each column of the data matrix. Here,  $R_1^{\text{DD}}(T)$  and  $R_1^{\text{SR}}(T)$  are the experimentally derived dipole–dipole and spin–rotation contributions to  $R_1$  in  $\text{H}_2\text{O}$ ,<sup>27</sup> scaled to  $x_{\text{H}} = 0.0098$ , assuming that  $R_1^{\text{DD}}$  is proportional to and  $R_1^{\text{SR}}$  is inversely proportional to the viscosity. The parameter  $c$  allows for a temperature-independent paramagnetic contribution. To limit the number of parameters, the SA contribution was not explicitly included in the smoothing function; its temperature dependence should be close to that of  $R_1^{\text{DD}}(T)$  and the small deviation can be absorbed by the three adjustable parameters. Clearly, with too many parameters, smoothing will have no effect. The smoothed  $R_1$

values, used for the subsequent  $B_0^2$  fit, were taken as the  $R_1$  values predicted by the smoothing function (with optimized parameters) at the nominal experimental temperatures. In most cases, the  $R_1$  correction effected by the smoothing protocol was within the estimated experimental uncertainty.

In modeling the time correlation function that governs SA relaxation (section 5), we make use of theoretical results on the symmetry properties of the configurationally averaged shielding tensor in liquid water. These results were derived from a set of 576 proton shielding tensors kindly supplied by Dr. Bernd G. Pfrommer. The shielding tensors were obtained by ab initio density functional theory (DFT) calculations<sup>25</sup> on a collection of periodically replicated water configurations taken from an ab initio molecular dynamics simulation<sup>36</sup> of 32 water molecules at 300 K and 1.0 g cm<sup>-3</sup>. In the original publication,<sup>25</sup> only results for the isotropic shielding were presented.

### 3. Magnetic Shielding Tensor

The magnetic induction field  $\mathbf{B}$  present at a nuclear site differs slightly from the uniform field  $\mathbf{B}_0$  applied to the sample. This is expressed as<sup>1</sup>

$$\mathbf{B} = (\mathbf{1} - \boldsymbol{\sigma})\mathbf{B}_0 \quad (1)$$

where  $\boldsymbol{\sigma}$  is the magnetic shielding tensor and  $\mathbf{1}$  is the unit tensor. The shielding tensor is of rank two and all its nine Cartesian components are in general independent. It can be decomposed into irreducible tensors of rank 0, 1, and 2:  $\boldsymbol{\sigma} = \boldsymbol{\sigma}^{(0)} + \boldsymbol{\sigma}^{(1)} + \boldsymbol{\sigma}^{(2)}$ , where<sup>37,38</sup>

$$\boldsymbol{\sigma}^{(0)} = \sigma_{\text{iso}}\mathbf{1} \quad (2)$$

$$\boldsymbol{\sigma}^{(1)} = (\boldsymbol{\sigma} - \boldsymbol{\sigma}^{\text{T}})/2 \quad (3)$$

$$\boldsymbol{\sigma}^{(2)} = (\boldsymbol{\sigma} + \boldsymbol{\sigma}^{\text{T}})/2 - \sigma_{\text{iso}}\mathbf{1} \quad (4)$$

where  $\boldsymbol{\sigma}^{\text{T}}$  denotes the transpose of the 3 x 3 matrix representation of the Cartesian tensor and

$$\sigma_{\text{iso}} \equiv \text{Tr } \boldsymbol{\sigma}/3 \quad (5)$$

For an isotropic liquid with rapidly tumbling molecules, only the scalar part  $\boldsymbol{\sigma}^{(0)}$  affects the NMR spectrum; accordingly, the so-called chemical shift of the resonance frequency is fully determined by the isotropic shielding  $\sigma_{\text{iso}}$ . The antisymmetric tensor  $\boldsymbol{\sigma}^{(1)}$ , which transforms under rotations as an axial vector, rarely makes significant contributions to observable properties (section 5). The traceless symmetric tensor  $\boldsymbol{\sigma}^{(2)}$  can be diagonalized by a rotation to a principal axes system. Because  $\boldsymbol{\sigma}^{(2)}$  is traceless, only two independent quantities can be formed from the three principal components  $\sigma_{11}$ ,  $\sigma_{22}$ , and  $\sigma_{33}$ . These are usually defined as the shielding anisotropy

$$\Delta\sigma \equiv \sigma_{33} - (\sigma_{11} + \sigma_{22})/2 \quad (6)$$

and the shielding asymmetry

$$\eta \equiv (\sigma_{22} - \sigma_{11})/\sigma_{33} \quad (7)$$

with the principal components labeled so that  $0 \leq \eta \leq 1$ . For

(34) Dietrich, W.; Bergmann, G.; Gerhards, R. *Z. Anal. Chem.* **1976**, *279*, 177–181.

(35) Press, W. H.; Teukolsky, S. A.; Vetterling, W. T.; Flannery, B. P. *Numerical Recipes in C*, 2nd Ed.; Cambridge University Press: Cambridge, 1992.

(36) Sprik, M.; Hutter, J.; Parrinello, M. *J. Chem. Phys.* **1996**, *105*, 1142–1152.

(37) Anet, F. A. L.; O’Leary, D. J. *Concepts Magn. Reson.* **1991**, *3*, 193–214; *ibid.*, **1992**, *4*, 35–52.

(38) Grant, D. M. In *Encyclopedia of Nuclear Magnetic Resonance*; Grant, D. M., Harris, R. K., Eds.; Wiley: Chichester, 1996; pp 1298–1321.

(nearly) axially symmetric shielding tensors ( $\eta \approx 0$ ), it is useful to define the components  $\sigma_{\parallel} \equiv \sigma_{33} + \sigma_{\text{iso}}$  and  $\sigma_{\perp} \equiv (\sigma_{11} + \sigma_{22})/2 + \sigma_{\text{iso}}$ , whereby eq 6 reads  $\Delta\sigma = \sigma_{\parallel} - \sigma_{\perp}$ .

Experimental information about the isotropic shielding  $\sigma_{\text{iso}}$  is usually obtained via the difference in observed resonance frequency relative to a reference state. The relative frequency difference, known as the chemical shift  $\delta$ , is related to the shielding through<sup>38</sup>

$$\delta = \sigma_{\text{iso}}^{\text{ref}} - \sigma_{\text{iso}} + (A - 1/3) (\kappa^{\text{ref}} - \kappa) \quad (8)$$

where  $\kappa$  is the magnetic (volume) susceptibility of the sample and the factor  $A$  depends on the shape and orientation of the sample ( $A = 1/3$  for a spherical sample). If the reference sample is a gas, the temperature dependence in  $\sigma_{\text{iso}}^{\text{ref}}$  and  $\kappa^{\text{ref}}$  can be neglected, and

$$\sigma_{\text{iso}}(T) = \sigma_{\text{iso}}(T^*) + \delta(T^*) - \delta(T) + (A - 1/3) [\kappa(T^*) - \kappa(T)] \quad (9)$$

This relation allows us to convert experimentally measured chemical shifts  $\delta(T)$  to absolute shieldings  $\sigma_{\text{iso}}(T)$ , provided that we know the shielding at one temperature  $T^*$ . The absolute proton shielding in liquid water has been determined with high accuracy at  $T^* = 34.7$  °C, where  $\sigma_{\text{iso}} = 25.790 \pm 0.014$  ppm.<sup>39</sup> We shall make use of data for the temperature-dependent proton chemical shift in H<sub>2</sub>O, with CH<sub>4</sub> gas as the reference sample.<sup>21</sup>

Our aim here is to determine the intermolecular contribution to the proton shielding tensor in liquid water. This intermolecular contribution fluctuates in time because of the motions of water molecules near the reference proton. Because these motions are much faster (by at least 8 orders of magnitude) than the resonance frequency variations that they induce, the observed chemical shift, and thus also the isotropic shielding, will be a thermal average over all (intermolecular and intramolecular) nuclear configurations. To emphasize this fact, we henceforth denote the configurationally averaged isotropic shielding by  $\langle \sigma_{\text{iso}} \rangle_V$ , where the subscript V signifies that the motions that average  $\sigma_{\text{iso}}$  are essentially (intra- and intermolecular) vibrations.

#### 4. Proton Spin Relaxation in Water

The longitudinal relaxation rate  $R_1 \equiv 1/T_1$  of the protons in a sample of bulk liquid H<sub>2</sub><sup>16</sup>O can be expressed as a sum of independent contributions from four relaxation mechanisms:<sup>1</sup>

$$R_1 = R_1^{\text{DD}} + R_1^{\text{SR}} + R_1^{\text{SA}} + R_1^{\text{PM}} \quad (10)$$

For pure H<sub>2</sub><sup>16</sup>O under ambient conditions, only  $R_1^{\text{DD}}$  makes a significant contribution. Its origin is the rotational modulation of the magnetic dipole–dipole (DD) coupling of the intramolecular proton pair and the translational (and rotational) modulation of DD couplings with protons in other water molecules. The spin–rotation contribution,  $R_1^{\text{SR}}$ , arises from the rotational modulation of the anisotropic coupling between the proton magnetic moment and the magnetic field induced by the rotating molecular charge distribution. For H<sub>2</sub><sup>16</sup>O,  $R_1^{\text{SR}}$  is less than 5% of  $R_1^{\text{DD}}$  at all temperatures within the liquid range (at atmospheric pressure). The temperature dependence in  $R_1^{\text{SR}}$  is essentially the inverse of that in the intramolecular part of

$R_1^{\text{DD}}$ .<sup>27,40</sup> The shielding anisotropy contribution,  $R_1^{\text{SA}}$ , is caused by rotational modulation of the anisotropic shielding tensor and will be considered in more detail in section 5. It scales as the square of the magnetic induction field  $B_0$ . For H<sub>2</sub><sup>16</sup>O,  $R_1^{\text{SA}}$  is negligible at typical NMR fields and only reaches 2% of  $R_1^{\text{DD}}$  at 18.8 T.

The paramagnetic contribution,  $R_1^{\text{PM}}$ , is caused by magnetic couplings between the water proton and unpaired electrons in impurities such as dissolved O<sub>2</sub> and transition metal ions (present in the water source or leached from Pyrex glass). To minimize  $R_1^{\text{PM}}$ , we have reduced the O<sub>2</sub> concentration by repeated pump–freeze–thaw cycles and reduced the contamination by paramagnetic ions by using a quartz tube and D<sub>2</sub>O with low paramagnetic content. Because we isolate  $R_1^{\text{SA}}$  from its field dependence, it is important that all other contributions are field-independent. This is true for  $R_1^{\text{DD}}$  and  $R_1^{\text{SR}}$  under the present (extreme motional narrowing) conditions, but  $R_1^{\text{PM}}$  may exhibit a potentially confounding field dependence (opposite to that in  $R_1^{\text{SA}}$ ). For example, the O<sub>2</sub>-induced contribution has dispersions at 40 MHz and 26 GHz.<sup>41</sup> In the frequency range (500–800 MHz) where  $R_1^{\text{SA}}$  makes substantial contributions to our  $R_1$  data,  $R_1^{\text{PM}}(\text{O}_2)$  is therefore essentially field-independent. (In this frequency range, the 40-MHz component contributes negligibly, while the 26-GHz component is in the extreme motional narrowing limit.) For water in equilibrium with air at room temperature,<sup>41</sup>  $R_1^{\text{PM}}(\text{O}_2) \approx 0.1$  s<sup>-1</sup>. However, the pump–freeze–thaw treatment presumably reduces  $R_1^{\text{PM}}(\text{O}_2)$  to a small fraction of this value. In any event, this residual paramagnetic contribution should not interfere with the determination of  $R_1^{\text{SA}}$ , since it is field independent.

The presence in water of the magnetic oxygen nuclide <sup>17</sup>O has two effects on the proton relaxation. First, the <sup>1</sup>H–<sup>17</sup>O DD coupling makes a contribution to  $R_1^{\text{DD}}$ , which has been used (in <sup>17</sup>O-enriched samples) to determine the rotational correlation time of the water molecule (section 6).<sup>30–32</sup> At the low natural abundance (0.037 atom %) of <sup>17</sup>O in our sample, this contribution is negligible. The second effect of <sup>17</sup>O is to introduce a contribution,  $R_1^{\text{SC}}$ , from so-called scalar relaxation induced by proton-exchange modulation of the electron-mediated spin–spin coupling  $J(^1\text{H}–^{17}\text{O}) = 80.6$  Hz.<sup>42–44</sup> In HDO, there is a similar  $R_1^{\text{SC}}$  contribution from the two-bond scalar coupling  $J(^1\text{H}–^2\text{H}) = 1.1$  Hz.<sup>44</sup> However, these scalar couplings do not contribute significantly to longitudinal relaxation at frequencies above ca. 10 kHz, where the dispersion of  $R_1^{\text{SC}}$  occurs (at neutral pH).<sup>45</sup> Like the shielding anisotropy, the isotropic shielding  $\sigma_{\text{iso}}$  also has a fluctuating intermolecular part that can induce spin relaxation. However, because the associated spin Hamiltonian (the Zeeman coupling) only involves the spin operator  $I_Z$ , it cannot contribute to  $R_1$ . (The contribution to the transverse rate  $R_2$  is expected to be 2–3 orders of magnitude smaller than  $R_1^{\text{SA}}$ .)

In a H<sub>2</sub>O/D<sub>2</sub>O mixture, intermolecular hydrogen exchange produces an essentially statistical distribution<sup>29,46</sup> of the isoto-

- (40) Hubbard, P. S. *Phys. Rev.* **1963**, *131*, 1155–1165.  
 (41) Teng, C.-L.; Hong, H.; Kühne, S.; Bryant, R. G. *J. Magn. Reson.* **2001**, *148*, 31–34.  
 (42) Meiboom, S. *J. Chem. Phys.* **1961**, *34*, 375–388.  
 (43) Halle, B.; Karlström, G. *J. Chem. Soc., Faraday Trans. 2* **1983**, *79*, 1031–1046.  
 (44) Sergeyev, N. M.; Sergeyeva, N. D.; Strelenko, Yu. A.; Raynes, W. T. *Chem. Phys. Lett.* **1997**, *277*, 142–146.  
 (45) Noack, F. *Prog. NMR Spectrosc.* **1986**, *18*, 171–276.

(39) Phillips, W. D.; Cooke, W. E.; Kleppner, D. *Phys. Rev. Lett.* **1975**, *35*, 1619–1622.

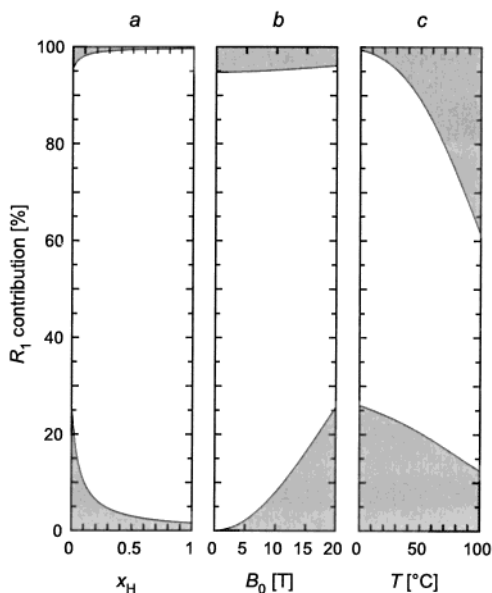


**Figure 1.** Relative contributions to water proton  $R_1$  from the shielding anisotropy (bottom, shaded), dipole–dipole (middle, white), and spin–rotation (upper, shaded) relaxation mechanisms versus (a) proton fraction  $x_H$  (at  $T = 27^\circ\text{C}$  and  $B_0 = 18.8\text{ T}$ ), (b) magnetic induction field  $B_0$  (at  $T = 27^\circ\text{C}$  and  $x_H = 0.01$ ), and (c) temperature  $T$  (at  $B_0 = 18.8\text{ T}$  and  $x_H = 0.01$ ). For this figure,  $R_1^{\text{DD}}$  and  $R_1^{\text{SR}}$  were taken from the literature<sup>27</sup> and corrected for the dynamic isotope effect according to the viscosity, whereas  $R_1^{\text{SA}}$  was calculated with the aid of eqs 22, 25, and 26.

polymers  $\text{H}_2\text{O}$ ,  $\text{D}_2\text{O}$ , and  $\text{HDO}$ . At room temperature and neutral pH, the hydrogen exchange time is about 1 ms,<sup>42,43</sup> 4–5 orders of magnitude shorter than the proton  $T_1$  measured here. The proton DD relaxation rate  $R_1^{\text{DD}}$  observed in a water sample with overall proton fraction  $x_H$  is therefore a population-weighted average over H–H and H–D pairs:<sup>29</sup>

$$R_1^{\text{DD}} = x_H R_1^{\text{DD}}(\text{H–H}) + (1 - x_H) R_1^{\text{DD}}(\text{H–D}) \quad (11)$$

Because the magnetogyric ratio  $\gamma_D$  of the deuteron is a factor 6.51 smaller than  $\gamma_H$  (and because of spin-dependent factors), DD relaxation is less efficient for an H–D pair than for an H–H pair. In fact, neglecting higher order isotope effects,  $R_1^{\text{DD}}(\text{H–D})/R_1^{\text{DD}}(\text{H–H}) = [4\gamma_D/(3\gamma_H)]^2 = 0.0419$ . By isotope dilution, the dominant  $R_1^{\text{DD}}$  term in eq 10 can thus be reduced by an order of magnitude, thereby allowing the much smaller  $R_1^{\text{SA}}$  term to be accurately determined. Also  $R_1^{\text{SA}}$  will be hydrogen-exchange averaged as in eq 11. However, here the isotope effects are of higher order and may safely be neglected. There is also a significant dynamic H/D isotope effect on  $R_1$ , which is essentially the same as the isotope effect on the viscosity (section 6).

Figure 1 shows the relative contributions to  $R_1$  from the DD, SR, and SA mechanisms, calculated with the aid of literature data and the results of the present work. As seen from Figure 1a, isotope dilution can enhance the relative contribution of  $R_1^{\text{SA}}$  to about 25% at a field of 18.8 T. The quadratic field dependence of  $R_1^{\text{SA}}$  is reflected in Figure 1b, while Figure 1c shows that  $R_1^{\text{SR}}$  can contribute as much as 40% at high temperatures and low proton fractions.

Equation 10 assumes that different relaxation mechanisms contribute additively to  $R_1$ . This is true only in the absence of

cross-correlations. A cross-correlation develops whenever two distinct spin couplings of the same tensor rank are (partly) modulated by the same molecular motion.<sup>1</sup> Cross-correlations open up new relaxation pathways, thereby inducing transient multispin order manifested, for example, as multiexponential magnetization recovery.<sup>47</sup> In the two-spin systems  $\text{H}_2^{16}\text{O}$  and  $\text{HD}^{16}\text{O}$ , a cross-correlation between the shielding anisotropy and (the intramolecular part of) the dipole–dipole coupling could potentially interfere with our determination of  $\Delta\sigma$ . It has even been proposed that  $\Delta\sigma$  could be determined (without isotope dilution) by observing the transient two-spin polarization modes induced by this cross-correlation.<sup>48</sup> This approach might work for water molecules dissolved in organic solvents but fails for bulk water because of the rapid proton exchange among water molecules. Any two-spin order induced by the cross-correlation will thus be quenched on a time scale much shorter than the observed relaxation time. Consequently, cross-correlations produce no observable effects in bulk water.

## 5. Time Correlation Function

In general, both the antisymmetric (rank 1) and symmetric (rank 2) parts of the shielding tensor contribute to the spin relaxation rate  $R_1^{\text{SA}}$ .<sup>37,49,50</sup> The ratio of these contributions is on the order of  $(\delta\sigma/\Delta\sigma)^2$ , where  $\delta\sigma \equiv (\sigma_{XY}^2 + \sigma_{XZ}^2 + \sigma_{YZ}^2)^{1/2}$  and the off-diagonal components refer to the full tensor in the principal frame of the symmetrized tensor. Ab initio DFT calculations<sup>25,33</sup> on liquid water (section 2) yield  $(\delta\sigma/\Delta\sigma)^2 = 3.3 \times 10^{-6}$ . We can therefore safely neglect the relaxation contribution from the antisymmetric shielding tensor.

In the extreme motional narrowing regime, where molecular tumbling is much faster than nuclear precession (as in the present study), the longitudinal proton spin relaxation rate induced by fluctuations in the symmetric shielding tensor is given by<sup>1,37,49</sup>

$$R_1^{\text{SA}} = (\gamma_H B_0)^2 J(0) \quad (12)$$

The zero-frequency spectral density  $J(0)$  is the integral of the time correlation function (TCF)  $G(\tau) = \langle \sigma_0^L(0) \sigma_0^L(\tau) \rangle$ , where  $\sigma_0$  is the  $N = 0$  irreducible spherical component of the shielding tensor in the lab-fixed frame.<sup>51</sup> This TCF can be decomposed as<sup>51</sup>

$$G(\tau) = \sum_{N=-2}^2 \sum_{P=-2}^2 \langle D_{0N}^{(2)}(\Omega(0)) [D_{0P}^{(2)}(\Omega_{\text{LS}}(\tau))]^* [\sigma_N^S(\xi(0))]^* \sigma_P^S(\xi(\tau)) \rangle \quad (13)$$

where  $D_{MN}^{(2)}(\Omega)$  is the rank-2 Wigner function and  $\Omega_{\text{LS}}$  denotes the Euler angles that effect the transformation from the lab-fixed frame (L) to the principal frame (S) of the symmetrized shielding tensor. Furthermore,  $\xi$  denotes the set of fluctuating geometrical variables responsible for the time dependence in the principal shielding components  $\sigma_N$ . If these components were time independent and if the Euler angles  $\Omega_{\text{LS}}$  were modulated by isotropic (spherical-top) rotational diffusion, then

$$G(\tau) = \frac{2}{15} (\Delta\sigma)^2 (1 + \eta^2/3) \exp(-6D_R\tau) \quad (14)$$

(47) Blicharski, J. S. *Phys. Lett.* **1967**, *24A*, 608–610.

(48) Werbelow, L. J. *Phys. Chem.* **1990**, *94*, 6663–6666.

(49) Blicharski, J. S. *Z. Naturforsch.* **1972**, *27a*, 1456–1458.

(50) Kowalewski, J.; Werbelow, L. J. *Magn. Reson.* **1997**, *128*, 144–148.

(51) Brink, D. M.; Satchler, G. R. *Angular Momentum*, 2nd ed.; Clarendon Press: Oxford, 1968.

(46) Sergeyev, N. M.; Sergeyeva, N. D.; Raynes, W. T. *J. Magn. Reson.* **1999**, *137*, 311–315.

with  $D_R$  the rotational diffusion coefficient. When this result is substituted into eq 12, we recover the standard expression for SA relaxation.<sup>1,37,49</sup> However, neither of the two approximations underlying eq 14 is expected to be quantitatively valid for the proton shielding in liquid water.

Ab initio calculations invariably yield a proton shielding tensor with near axial symmetry; this is true for the isolated water molecule ( $\eta = 0.04$ ),<sup>52</sup> for ice-like water clusters ( $\eta = 0.005$ )<sup>53</sup> and for liquid water ( $\eta = 0.10 \pm 0.01$ ).<sup>25,33</sup> Solid-state NMR data from ice Ih are also consistent with an axially symmetric shielding tensor.<sup>54–56</sup> As seen from eq 14, such a small asymmetry parameter does not affect the TCF significantly. If the assumption of isotropic rotation is relaxed, a term linear in  $\eta$  appears, but if the rotation is only moderately anisotropic (as seems to be the case<sup>57</sup>), this term will be negligibly small. To an excellent approximation, we can therefore set  $\eta = 0$ . It then follows that  $\sigma_N = \delta_{N0}\sigma_0 = \delta_{N0}\sqrt{2/3}\Delta\sigma$ , and eq 13 reduces to

$$G(\tau) = \frac{2}{3}\langle P_2(\zeta(0))P_2(\zeta(\tau))\Delta\sigma(\xi(0))\Delta\sigma(\xi(\tau)) \rangle \quad (15)$$

where  $\zeta = \cos \theta_{LS}$ .

Ab initio DFT calculations<sup>25,33</sup> on liquid water (section 2) show that the principal (S) frame of the shielding tensor never departs more than a few degrees from a molecule-fixed frame with the unique axis (corresponding to the most shielded component  $\sigma_{33}$ ) along the covalent O–H bond. This is also the case for the isolated water molecule and the water dimer.<sup>5</sup> The stochastic variable  $\zeta$  therefore describes the orientation of the O–H bond. The time dependence in  $\Delta\sigma$  is caused by fluctuations in the intramolecular geometry (primarily the O–H bond length) and in the intermolecular geometry (primarily the hydrogen bond length and angle). The characteristic time scales for these fluctuations, estimated as  $(2\pi c\bar{\nu})^{-1}$  with  $\bar{\nu}$  the center frequency (in wavenumber units) of the corresponding infrared or Raman band in liquid H<sub>2</sub>O at room temperature,<sup>58–60</sup> are 2 fs (O–H stretch) and 5–100 fs (librations and hindered translations). The fast librational motions give rise to a nonexponential initial decay in the purely rotational TCF that is obtained by setting  $\Delta\sigma = 1$  in eq 15. This so-called glitch reduces the TCF by 10–20% within the first 100–200 fs, whereupon the TCF decays exponentially with a rotational correlation time  $\tau_R$  of about 2 ps (at room temperature). This general behavior is seen in all molecular dynamics simulations, whether they are based on classical<sup>61–63</sup> or quantum-mechanical<sup>36,64</sup> force fields.

To separate the effects of the fast vibrational and slow rotational motions on the TCF, we introduce an intermediate

frame V, defined as the principal frame of the vibrationally averaged (axially symmetric) shielding tensor. The symmetry axis of the V frame should coincide closely with the orientation of the librationally averaged O–H bond. Because the vibrational motions associated with the variables  $\zeta_{VS}$  and  $\xi$  are much faster than molecular rotation, associated with  $\zeta_{LV}$ , the TCF in eq 15 can be split in two independent parts without any cross-term.<sup>65,66</sup> Taking the time integral of this TCF, we obtain for the spectral density that appears in eq 12,

$$J(0) = \frac{2}{15}\langle P_2(\zeta_{VS})\Delta\sigma(\xi) \rangle_V^2 \tau_R + J_{\text{fast}}(0) \quad (16)$$

where  $\langle \dots \rangle$  denotes a vibrational average over the fast variables  $\zeta_{VS}$  and  $\xi$ . In eq 16, we have defined

$$\tau_R \equiv 5 \int_0^\infty d\tau \langle P_2(\zeta_{LV}(0))P_2(\zeta_{LV}(\tau)) \rangle \quad (17)$$

and

$$J_{\text{fast}}(0) \equiv \int_0^\infty d\tau [G(\tau) - G_{\text{slow}}(\tau)] \quad (18)$$

where  $G_{\text{slow}}(\tau)$  is the TCF that, when integrated over time, yields the first term in eq 16.

Equation 16 is in a form suitable for introducing two approximations. First, we neglect the spectral density contribution  $J_{\text{fast}}(0)$  from the fast motions. To show that this is permissible, we assume that the fast and slow partial TCFs decay exponentially with correlation times  $\tau_V$  and  $\tau_R$ , respectively. One can then show that

$$\frac{J_{\text{fast}}(0)}{J(0)} = \left(1 + \frac{1 + \tau_R/\tau_V}{A^{-2} - 1}\right)^{-1} \quad (19)$$

where  $A = \langle P_2(\zeta_{VS})\Delta\sigma(\xi) \rangle_V / \langle [P_2(\zeta_{VS})\Delta\sigma(\xi)]^2 \rangle_V^{1/2}$ . Clearly,  $J_{\text{fast}}(0)$  will be negligible if the motions are time-scale separated ( $\tau_V \ll \tau_R$ ) and/or the vibrational amplitude is small ( $A \approx 1$ ). For  $\tau_V/\tau_R = 0.1$  (see above) and  $A = 0.96$  (from ab initio DFT calculations; see section 2),<sup>25,33</sup> eq 19 shows that  $J_{\text{fast}}(0)$  contributes merely 0.8% of  $J(0)$ .

The second approximation that we shall introduce in eq 16 is to factorize the vibrational average as

$$\langle P_2(\zeta_{VS})\Delta\sigma(\xi) \rangle_V = \langle P_2(\zeta_{VS}) \rangle_V \langle \Delta\sigma(\xi) \rangle_V \quad (20)$$

The difference between the left and right members is

$$\int d\zeta_{VS} \int d\xi f(\zeta_{VS}, \xi) [P_2(\zeta_{VS}) - \langle P_2(\zeta_{VS}) \rangle_V] \Delta\sigma(\xi) \quad (21)$$

where  $f(\zeta_{VS}, \xi)$  is the joint equilibrium distribution for the fast variables. If this distribution is narrow in  $\zeta_{VS}$ , as we expect, then  $P_2(\zeta_{VS})$  will never deviate much from  $\langle P_2(\zeta_{VS}) \rangle_V$ . The integral in eq 21 will therefore be small even if  $\zeta_{VS}$  and  $\xi$  are partially correlated. In fact, ab initio DFT calculations (section 2) show that the two members of eq 20 differ by only 2%.<sup>25,33</sup>

- (52) Vaara, J.; Lounila, J.; Ruud, K.; Helgaker, T. *J. Chem. Phys.* **1998**, *109*, 8388–8397.  
 (53) Hinton, J. F.; Guthrie, P.; Pulay, P.; Wolinski, K. *J. Am. Chem. Soc.* **1992**, *114*, 1604–1605.  
 (54) Pines, A.; Ruben, D. J.; Vega, S.; Mehring, M. *Phys. Rev. Lett.* **1976**, *36*, 110–113.  
 (55) Ryan, L. M.; Wilson, R. C.; Gerstein, B. C. *Chem. Phys. Lett.* **1977**, *52*, 341–344.  
 (56) Burum, D. P.; Rhim, W. K. *J. Chem. Phys.* **1979**, *70*, 3553–3554. (b) Rhim, W. K.; Burum, D. P.; Elleman, D. D. *J. Chem. Phys.* **1979**, *71*, 3139–3141.  
 (57) Ropp, J.; Lawrence, C.; Farrar, T. C.; Skinner, J. L. *J. Am. Chem. Soc.* **2001**, *123*, 8047–8052.  
 (58) Walrafen, G. E. In *Water: a Comprehensive Treatise*, Franks, F., Ed.; Plenum: New York, 1972; Vol. 1, Chapter 5.  
 (59) Silvestrelli, P. L.; Bernasconi, M.; Parrinello, M. *Chem. Phys. Lett.* **1997**, *277*, 478–482.  
 (60) Bursulaya, B. D.; Kim, H. J. *J. Chem. Phys.* **1998**, *109*, 4911–4919.

- (61) Impey, R. W.; Madden, P. A.; McDonald, I. R. *Mol. Phys.* **1982**, *46*, 513–539.  
 (62) Svishchev, I. M.; Kusalik, P. G. *J. Phys. Chem.* **1994**, *98*, 728–733.  
 (63) Yeh, Y.-L.; Mou, C.-Y. *J. Phys. Chem. B* **1999**, *103*, 3699–3705.  
 (64) Bursulaya, B. D.; Jeon, J.; Zichi, D. A.; Kim, H. J. *J. Chem. Phys.* **1998**, *108*, 3286–3295.  
 (65) Halle, B.; Wennerström, H. *J. Chem. Phys.* **1981**, *75*, 1928–1943.  
 (66) Cummins, P. L.; Bacskay, G. B.; Hush, N. S.; Halle, B.; Engström, S. J. *Chem. Phys.* **1985**, *82*, 2002–2013.

After these two approximations, eq 16 is inserted into eq 12 to give

$$R_1^{\text{SA}} = \frac{2}{15}(\gamma B_0)^2 \langle \Delta\sigma \rangle_V^2 \tau_R^{\text{eff}} \quad (22)$$

where we have also introduced the effective correlation time

$$\tau_R^{\text{eff}} = \langle P_2(\xi) \rangle^2 \tau_R \quad (23)$$

defined as the time integral of the reduced TCF  $G(\tau)/G(0)$  with  $G(\tau)$  given by eq 15.

## 6. Rotational Correlation Time

To extract  $\langle \Delta\sigma \rangle_V$  from the measured  $R_1^{\text{SA}}$ , we must know the effective rotational correlation time  $\tau_R^{\text{eff}}$  in eq 22. This quantity can be obtained from the proton relaxation rate contribution  $R_1^{\text{DD}}(^1\text{H}-^{17}\text{O})$  induced by the intramolecular  $^1\text{H}-^{17}\text{O}$  dipole–dipole coupling in  $^{17}\text{O}$ -enriched water. Because the symmetry axis of the principal shielding tensor is essentially collinear with the O–H bond (section 5),  $R_1^{\text{SA}}$  and  $R_1^{\text{DD}}(^1\text{H}-^{17}\text{O})$  involve exactly the same effective rotational correlation time,  $\tau_R^{\text{eff}}$ . The treatment of vibrational averaging presented in section 5 is applicable also to  $R_1^{\text{DD}}(^1\text{H}-^{17}\text{O})$  if the shielding anisotropy  $\Delta\sigma$  is replaced by  $r^{-3}_{\text{OH}}$ , with  $r_{\text{OH}}$  the covalent O–H bond length. We thus have<sup>1,30</sup>

$$R_1^{\text{DD}}(^1\text{H}-^{17}\text{O}) = \frac{35}{3} \left( \frac{\mu_0}{4\pi} \hbar \gamma_{\text{H}} \gamma_{\text{O}} \right)^2 \langle r_{\text{OH}}^{-3} \rangle_V^2 \tau_R^{\text{eff}} \quad (24)$$

It is important to note that, as long as the principal axis of the shielding tensor is collinear with the O–H bond, the effective correlation times  $\tau_R^{\text{eff}}$  in eqs 22 and 24 are identical even if the rotational motion is anisotropic. To estimate the effect of a small misalignment of the SA and DD tensors, we assume that the water molecule behaves as a rigid symmetric top. We then derive an expression for the ratio of the effective correlation times in eqs 22 and 24 which involves three parameters: the ratio  $D_{\parallel}/D_{\perp}$  of the principal rotational diffusion coefficients, the angle  $\theta_{\text{SA}}$  between the symmetry axes of the diffusion and shielding tensors, and the angle  $\theta_{\text{DD}}$  between the symmetry axis of the diffusion tensor and the O–H bond. For  $D_{\parallel}/D_{\perp} = 1.5$  (according to a recent study,<sup>57</sup> the ratio of the rotational correlation times of the O–H bond and the normal to the plane of the water molecule is 1.33) and  $|\theta_{\text{SA}} - \theta_{\text{DD}}| < 10^\circ$ , we thus find that the effective correlation times  $\tau_R^{\text{eff}}$  in eqs 22 and 24 differ by less than 3% (and less than 1% if the symmetry axis of the diffusion tensor is near the O–H bond). It should also be noted that, in our treatment, the effect of vibrational averaging is partitioned in two factors: the angular factor  $\langle P_2(\xi_{\text{VS}}) \rangle$  in eq 23 and the vibrationally averaged interaction constants  $\langle \Delta\sigma \rangle_V$  and  $\langle r_{\text{OH}}^{-3} \rangle_V$  in eqs 22 and 24. This partitioning is convenient because the orientational order parameter  $\langle P_2(\xi_{\text{VS}}) \rangle$ , which is not accurately known, is the same for SA and DD relaxation (given that the principal axes coincide) and therefore cancels out in our analysis. Interaction constants deduced from solid-state NMR line shape analysis, on the other hand, incorporate the orientational order parameter (as in eq 20).<sup>67,68</sup>

(67) Henry, E. R.; Szabo, A. *J. Chem. Phys.* **1985**, *82*, 4753–4761.

(68) Ishii, Y.; Terao, T.; Hayashi, S. *J. Chem. Phys.* **1997**, *107*, 2760–2774.

To obtain the correlation time  $\tau_R^{\text{eff}}$  from the measured  $R_1^{\text{DD}}(^1\text{H}-^{17}\text{O})$ , we only need the vibrational average  $\langle r_{\text{OH}}^{-3} \rangle_V$ . Time-of-flight neutron scattering measurements at high momentum transfers yield  $\langle r_{\text{OD}} \rangle_V = 0.970(2)$  Å for the mean O–D bond length in liquid  $\text{D}_2\text{O}$ , with no significant variation in the temperature range 25–200 °C.<sup>69</sup> The root-mean-square bond length variation (essentially due to zero-point vibrations) is  $\sigma_{\text{OD}} = 0.059$  Å, likewise temperature independent.<sup>69</sup> Virtually the same bond length is obtained in  $\text{D}_2\text{O}$  vapor by either electron diffraction,  $\langle r_{\text{OD}} \rangle_V = 0.970(2)$  Å and  $\sigma_{\text{OD}} = 0.056(2)$  Å<sup>70</sup> or quantum-mechanical analysis of vibration spectra,  $\langle r_{\text{OD}} \rangle_V = 0.971(1)$  Å.<sup>71,72</sup> Since there is no significant difference in bond length between vapor and liquid, the slightly longer bond in  $\text{H}_2\text{O}$  vapor, with  $\langle r_{\text{OH}} \rangle_V = 0.976(1)$  Å and  $\sigma_{\text{OH}} = 0.067$  Å,<sup>70–72</sup> may be taken to apply also to liquid  $\text{H}_2\text{O}$ . Averaging  $r_{\text{OH}}^{-3}$  over a Gaussian distribution (as expected for the zero-point vibration) with  $\langle r_{\text{OH}} \rangle_V = 0.976$  Å and  $\sigma_{\text{OH}} = 0.067$  Å, we find  $\langle r_{\text{OH}}^{-3} \rangle_V^{-1/3} = 0.967$  Å.

We can now deduce  $\tau_R^{\text{eff}}$  from eq 24 by inserting  $\langle r_{\text{OH}}^{-3} \rangle_V^{-1/3} = 0.967$  Å and values for the physical constants and using previously reported<sup>31,32</sup>  $R_1^{\text{DD}}(^1\text{H}-^{17}\text{O})$  data covering the temperature range from –11 to 65 °C, corrected for an estimated 2% intermolecular contribution and for the small oxygen isotope effect on  $\tau_R^{\text{eff}}$  (assumed to scale as the viscosity).<sup>30</sup> We thus find that  $\tau_R^{\text{eff}}$  is very nearly proportional to  $\eta(T)/T$ , where  $\eta$  is the bulk  $\text{H}_2\text{O}$  viscosity,<sup>73</sup> as expected for a hydrodynamic rotation model. To account for the 10% linear deviation from  $\eta(T)/T$  scaling, we represent  $\tau_R^{\text{eff}}$  as

$$\tau_R^{\text{eff}}/\text{ps} = 480[\eta(T)/\text{cP}][1/(T/\text{K}) + 9.20 \times 10^{-4}] \quad (25)$$

This function is shown in Figure 2 along with the experimental data. We believe that this expression provides the most accurate estimate currently available for the effective rotational correlation time of the O–H bond in  $\text{H}_2\text{O}$ . At 25 °C, it yields  $\tau_R^{\text{eff}} = 1.83$  ps, with an estimated uncertainty of  $\pm 0.05$  ps. Because  $\tau_R^{\text{eff}}$  is defined as the integral of the normalized TCF, it incorporates the effect of the initial (<0.2 ps) glitch in the TCF (section 5). Beyond the glitch, the TCF decays with a somewhat longer (10–20%, judging from typical simulation-derived glitch amplitudes) time constant.

The correlation time given by eq 25 pertains to an O–H bond in pure  $\text{H}_2\text{O}$  and can therefore not be equated with  $\tau_R^{\text{eff}}$  for our  $R_1^{\text{SA}}$  data, which refer to an O–H bond in a HDO molecule surrounded by  $\text{D}_2\text{O}$  molecules. The reverse situation occurs for deuteron relaxation in  $\text{H}_2\text{O}/\text{D}_2\text{O}$  mixtures, because  $R_1(^2\text{H})$  always monitors the rotational dynamics of an O–D bond. To an excellent approximation, the electric field gradient tensor responsible for the  $^2\text{H}$  relaxation is axially symmetric and collinear with the O–D bond.<sup>66</sup> Although the correlation time to be used with  $R_1^{\text{SA}}$  could have been derived from  $R_1(^2\text{H})$ , this approach is less accurate, since the quadrupole coupling constant has not been directly determined experimentally for liquid water

(69) Ichikawa, K.; Kameda, Y.; Yamaguchi, T.; Wakita, H.; Misawa, M. *Mol. Phys.* **1991**, *73*, 79–86.

(70) Shibata, S.; Bartell, L. S. *J. Chem. Phys.* **1965**, *42*, 1147–1151.

(71) Polyansky, O. L.; Jensen, P.; Tennyson, J. *J. Chem. Phys.* **1996**, *105*, 6490–6497.

(72) Wigglesworth, R. D.; Raynes, W. T.; Sauer, S. P. A.; Oddershede, J. *Mol. Phys.* **1999**, *96*, 1595–1607.

(73) *Revised Release on the IAPS Formulation 1985 for the Viscosity of Ordinary Water Substance*; International Association for the Properties of Water and Steam, 1997.

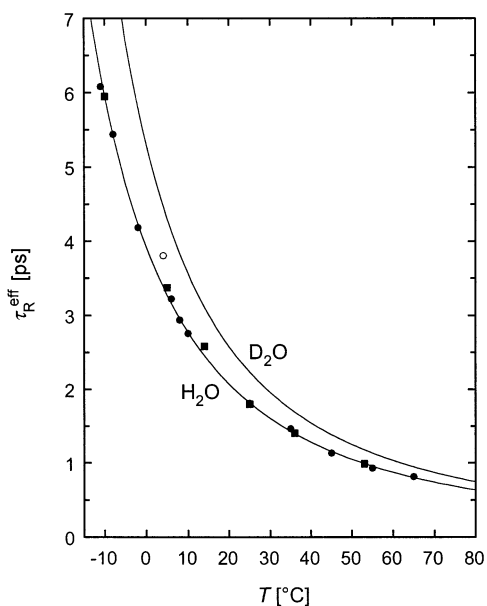


**Figure 2.** Effective second-rank rotational correlation time for the O–H bond in H<sub>2</sub>O versus temperature. The data points were obtained from  $R_1^{\text{DD}}(\text{H}-^{17}\text{O})$  data reported by Struis et al. (squares)<sup>31</sup> and by Ludwig et al. (circles),<sup>32</sup> using  $\langle r_{\text{OH}}^{-3} \rangle^{-1/3} = 0.967 \text{ \AA}$ . The H<sub>2</sub>O curve resulted from a fit to the data points (excluding the outlier indicated with an open circle) according to eq 25. The D<sub>2</sub>O curve was then obtained by viscosity scaling.

and since it appears to have a small but significant temperature dependence.<sup>32</sup> It has been shown that  $R_1(^2\text{H})$  varies linearly with the proton fraction  $x_{\text{H}}$ ,<sup>30</sup> which is also the case for the viscosity.<sup>74</sup> Moreover,  $R_1(^2\text{H}; \text{D}_2\text{O})/R_1(^2\text{H}; \text{H}_2\text{O}) = 1.218 \pm 0.002$  at 25 °C,<sup>30</sup> which is very close to the viscosity ratio  $\eta(\text{D}_2\text{O})/\eta(\text{H}_2\text{O}) = 1.230$  at 25 °C.<sup>73,75</sup> To an excellent approximation, we can therefore obtain  $\tau_{\text{R}}^{\text{eff}}$  in any H<sub>2</sub>O/D<sub>2</sub>O mixture by inserting in eq 25 the viscosity for that mixture, calculated as  $\eta(T, x_{\text{H}}) = x_{\text{H}}\eta(T; \text{H}_2\text{O}) + (1 - x_{\text{H}})\eta(T; \text{D}_2\text{O})$ .

## 7. Determination of the Shielding Anisotropy

We measured the proton longitudinal relaxation rate  $R_1$  at nine temperatures from 0 °C (below the 3.8 °C freezing point of D<sub>2</sub>O) to 80 °C and at five magnetic induction fields  $B_0$  in the range 2.35–18.8 T. Figure 3 shows the results from the lowest and highest fields. Because  $R_1^{\text{SA}}$  is the only field-dependent contribution to  $R_1$ , the difference between the curves in Figure 3 can be entirely attributed to relaxation by the SA mechanism. The temperature dependence in  $R_1^{\text{SA}}$  is mainly due to  $\tau_{\text{R}}^{\text{eff}}$ , which varies by a factor 7 over the investigated temperature range (Figure 2), while  $\langle \Delta\sigma \rangle_{\text{V}}^2$  varies by only 30% over the same range (see below). Highly accurate  $R_1$  data are therefore needed to determine the temperature dependence in  $\langle \Delta\sigma \rangle_{\text{V}}$ . To improve the accuracy, we used a smoothing protocol based on the expected functional form of the temperature dependence in  $R_1$  (section 2). For the subsequent analysis, we thus used  $R_1$  values determined by the curves in Figure 3 at the experimental temperatures. Whereas the 18.8 T data are hardly affected by the smoothing procedure, it is clear that the 40 °C point at 2.35 T is slightly in error.

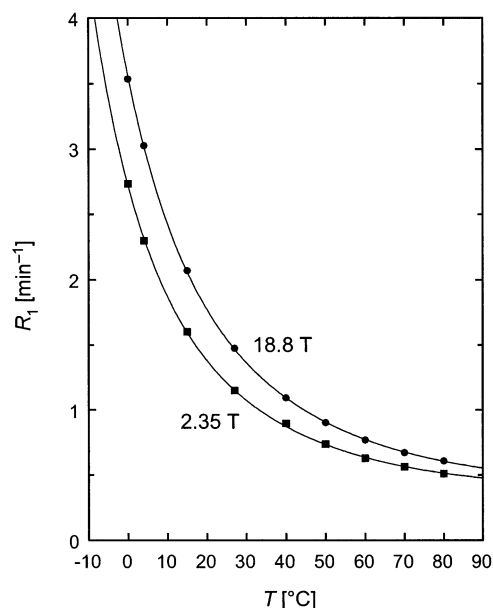


**Figure 3.** Water proton  $R_1$  versus temperature for a water sample with  $x_{\text{H}} = 0.0098$ , measured at magnetic induction fields  $B_0 = 2.35 \text{ T}$  (squares) and 18.8 T (circles). The curves are smoothing functions as described in the text.

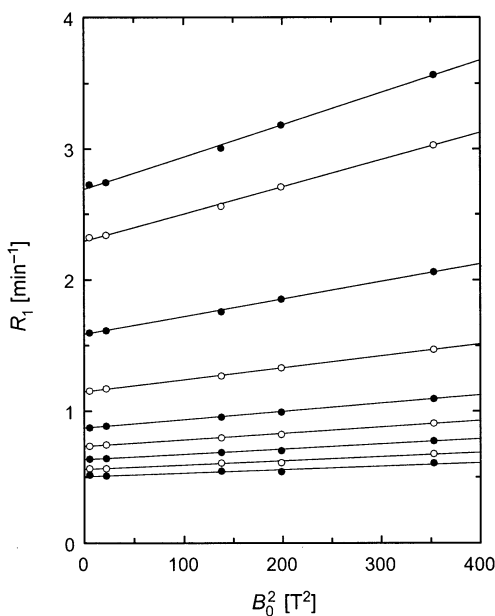


**Figure 4.** Water proton  $R_1$  versus the square of the magnetic induction field  $B_0$  for a water sample with  $x_{\text{H}} = 0.0098$ , measured at (from top to bottom) 0, 4, 15, 27, 40, 50, 60, 70, and 80 °C. The  $R_1$  data have been subjected to temperature smoothing, as shown in Figure 3. The lines resulted from linear least-squares fits.

In Figure 4, we have plotted the smoothed  $R_1$  data versus the square of the magnetic induction field. As expected from eqs 10 and 22,  $R_1$  increases linearly with  $B_0^2$ . Dividing the slope, proportional to  $\langle \Delta\sigma \rangle_{\text{V}}^2 \tau_{\text{R}}^{\text{eff}}$ , by the correlation time  $\tau_{\text{R}}^{\text{eff}}$ , calculated from eq 25 with the viscosity at the experimental temperature and  $x_{\text{H}} = 0.0098$ , we obtain the vibrationally averaged shielding anisotropy  $\langle \Delta\sigma \rangle_{\text{V}}$  shown in Figure 5. The temperature dependence of  $\langle \Delta\sigma \rangle_{\text{V}}$  is linear within the experimental accuracy, with

$$\langle \Delta\sigma \rangle_{\text{V}}/\text{ppm} = 28.54 - 0.0432(T/\text{°C}) \quad (26)$$

(74) Kestin, J.; Imaishi, N.; Nott, S. H.; Nieuwoudt, J. C.; Sengers, J. V. *Physica A* **1985**, *134*, 38–58.

(75) *Release on Viscosity and Thermal Conductivity of Heavy Water Substance*; International Association for the Properties of Steam: Erlangen, Germany, 1984.

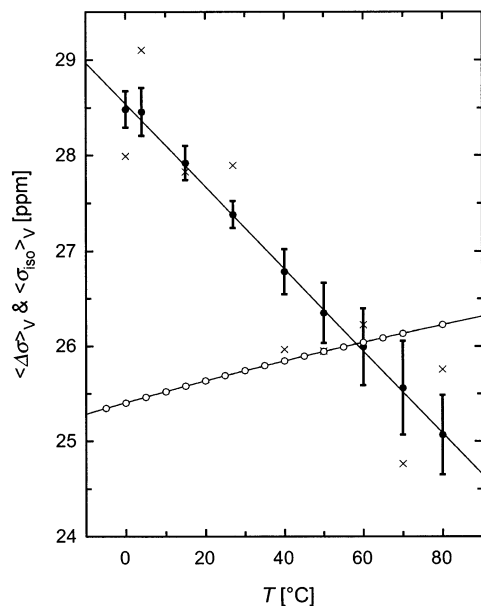


**Figure 5.** Temperature dependence of the vibrationally averaged proton shielding anisotropy  $\langle \Delta\sigma \rangle_V$  (solid circles) and isotropic shielding  $\langle \sigma_{iso} \rangle_V$  (open circles) in liquid water. The shielding anisotropy obtained without temperature smoothing is also shown (crosses). The isotropic shielding was obtained by converting published<sup>21</sup> chemical shifts to an absolute shielding scale by means of eq 9. The curves represent eqs 26 and 27.

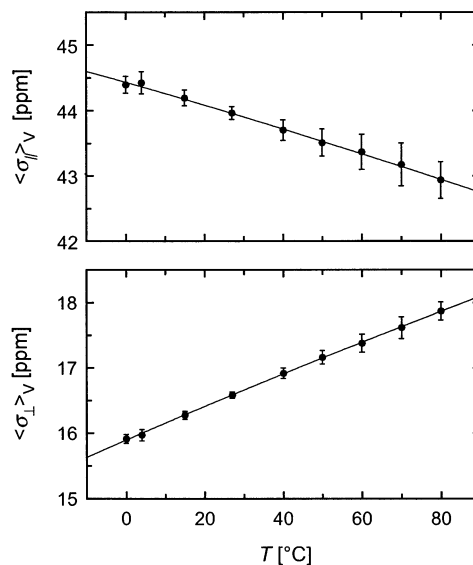
The  $\langle \Delta\sigma \rangle_V$  values obtained without data smoothing are included in Figure 5; the scatter is larger, but the slope and intercept are not affected much.

Figure 5 also shows the vibrationally averaged isotropic shielding  $\langle \sigma_{iso} \rangle_V$ , obtained from eq 9 and Hindman's chemical shift measurements on H<sub>2</sub>O.<sup>21</sup> For the small susceptibility correction in eq 9, we used  $A = 1/2$ , as appropriate for a long cylindrical sample with the cylinder axis perpendicular to the  $B_0$  field,<sup>21</sup> and  $\kappa(T) = \chi_m(T)\rho(T)/M$ , with the molar susceptibility<sup>76</sup>  $\chi_m(T) = -4\pi [12.93 + 0.0016(T/^\circ\text{C})] \times 10^{-6} \text{ cm}^3 \text{ mol}^{-1}$ , mass density<sup>77</sup>  $\rho(T)$ , and molar mass  $M$  of H<sub>2</sub>O. Although the susceptibility contribution to the measured chemical shift is quite large,  $\kappa/6 = 1.5 \text{ ppm}$ , it is only weakly temperature dependent. The susceptibility correction in eq 9 is therefore very small, ranging from  $-26$  to  $+4 \text{ ppb}$  within the temperature range  $0$ – $80 \text{ }^\circ\text{C}$ . The isotropic shielding in the range  $-15$  to  $100 \text{ }^\circ\text{C}$  is accurately represented by a cubic polynomial in  $T/^\circ\text{C}$ :

$$\langle \sigma_{iso} \rangle_V / \text{ppm} = (25.406 + 1.188 \times 10^{-2})T - (2.63 \times 10^{-5})T^2 + (7.1 \times 10^{-8})T^3 \quad (27)$$

The temperature dependence in the shielding anisotropy  $\langle \Delta\sigma \rangle_V$  is opposite to that in  $\langle \sigma_{iso} \rangle_V$  and four times stronger:  $d\langle \Delta\sigma \rangle_V / dT = -43.2 \text{ ppb K}^{-1}$  and  $d\langle \sigma_{iso} \rangle_V / dT = +10.7 \text{ ppb K}^{-1}$  (at  $25 \text{ }^\circ\text{C}$ ). The shielding anisotropy is therefore a more sensitive probe of temperature-dependent water structure.

It should be noted that, although  $\langle \sigma_{iso} \rangle_V$  was determined in H<sub>2</sub>O and  $\langle \Delta\sigma \rangle_V$  in 99% D<sub>2</sub>O, both refer to protons in O–H $\cdots$ O hydrogen bonds. Because even the primary isotope effect on the shielding, i.e., the difference between O–H $\cdots$ O and O–D $\cdots$ O, is small (typically  $<0.2 \text{ ppm}$ ), the secondary isotope effect of relevance here can safely be neglected. High-level ab



**Figure 6.** Temperature dependence of the vibrationally averaged principal components  $\langle \sigma_{||} \rangle_V$  and  $\langle \sigma_{\perp} \rangle_V$  parallel and perpendicular to the O–H bond, derived from the results in Figure 5.

initio calculations on the isolated water molecule yield a primary isotope effect of  $0.14 \text{ ppm}$  in  $\langle \sigma_{iso} \rangle_V$  and  $0.29 \text{ ppm}$  in  $\langle \Delta\sigma \rangle_V$ , while the secondary (intramolecular) isotope effect is  $0.04 \text{ ppm}$  in  $\langle \sigma_{iso} \rangle_V$  and  $0.004 \text{ ppm}$  in  $\langle \Delta\sigma \rangle_V$ .<sup>52,72</sup> In Figure 5,  $\langle \sigma_{iso} \rangle_V$  and  $\langle \Delta\sigma \rangle_V$  can thus both be regarded as pertaining to H<sub>2</sub>O.

By taking linear combinations of  $\langle \Delta\sigma \rangle_V$  and  $\langle \sigma_{iso} \rangle_V$ , we can now obtain the shielding components  $\langle \sigma_{||} \rangle_V$  and  $\langle \sigma_{\perp} \rangle_V$  parallel and perpendicular to the symmetry axis of the shielding tensor, which is nearly collinear with the O–H bond (section 5). As seen from Figure 6, both components vary essentially linearly over the investigated temperature range. The slopes are (at  $25 \text{ }^\circ\text{C}$ )  $d\langle \sigma_{||} \rangle_V / dT = -18.1 \text{ ppb K}^{-1}$  and  $d\langle \sigma_{\perp} \rangle_V / dT = +25.1 \text{ ppb K}^{-1}$ . In the shielding anisotropy,  $\langle \Delta\sigma \rangle_V = \langle \sigma_{||} \rangle_V - \langle \sigma_{\perp} \rangle_V$ , the opposite temperature variations of  $\langle \sigma_{||} \rangle_V$  and  $\langle \sigma_{\perp} \rangle_V$  add constructively, whereas in  $\langle \sigma_{iso} \rangle_V = (\langle \sigma_{||} \rangle_V + 2\langle \sigma_{\perp} \rangle_V) / 3$ , they partly cancel, thus accounting for the much stronger observed temperature dependence in  $\langle \Delta\sigma \rangle_V$  as compared to  $\langle \sigma_{iso} \rangle_V$  (Figure 5).

Ab initio calculations on the water dimer demonstrate that hydrogen bonding affects the proton shielding tensor by two principal mechanisms.<sup>5</sup> An essentially isotropic deshielding results from the reduced electron density on the hydrogen atom. In addition, there is an important contribution from the magnetic field at the proton site generated by currents induced by the applied magnetic field in the electron distribution at the acceptor oxygen. This acceptor effect is responsible for the opposite hydrogen-bond shifts in  $\sigma_{||}$  and  $\sigma_{\perp}$ . As a result, the hydrogen-bond shift in  $\Delta\sigma$  is strongly dominated by the acceptor effect, whereas the hydrogen-bond shift in  $\sigma_{iso}$  has equal (and much smaller) contributions from the acceptor effect and the electron depletion effect.<sup>5</sup> These and other<sup>25,33</sup> theoretical results indicate that variations in hydrogen-bond geometry in liquid water will be more strongly manifested in the shielding anisotropy than in the isotropic chemical shift, in accordance with the present experimental findings.

## 8. Magnetic Shielding and Intermolecular Interactions

The isolated water molecule in dilute vapor and the optimally hydrogen bonded water molecule in ice Ih are the obvious

(76) Landolt-Börnstein, *New series*; Springer-Verlag: Berlin, 1986; Vol. II: 16, *Diamagnetic Susceptibility*.

(77) Kell, G. S. *J. Chem. Engin. Data* **1967**, *12*, 66.

benchmarks for an analysis of interaction effects on the proton shielding tensor in liquid water.

The most accurate results for the isolated water molecule have come from high-level *ab initio* calculations,<sup>52</sup> yielding  $\langle\sigma_{\text{iso}}\rangle_V = 30.2$  ppm and  $\langle\Delta\sigma\rangle_V = 19.1$  ppm with an estimated uncertainty of  $\pm 0.1$  ppm due to basis set incompleteness and approximations in the treatment of electron correlation. These results incorporate zero-point rovibrational averaging. Since the intramolecular vibrational modes are hardly excited in the temperature range (0–100 °C) of interest here, the shielding tensor in the isolated water molecule may be taken to be independent of temperature. (On going from 0 to 300 K,  $\langle\sigma_{\text{iso}}\rangle_V$  and  $\langle\Delta\sigma\rangle_V$  decrease by 26 and 46 ppb, respectively.<sup>52</sup>) The often quoted experimental value  $\langle\sigma_{\text{iso}}\rangle_V = 30.052 \pm 0.015$  ppm is not as accurate as indicated. It was derived<sup>78</sup> in a rather indirect manner from the measured vapor-to-liquid shift,<sup>21</sup> which involves a large (1.5 ppm) susceptibility correction (see eq 8). In making this correction, the geometrical *A* factor was set equal to 1/2, which is strictly valid only for an infinitely long cylinder.<sup>79</sup> If the finite sample height is taken into account, *A* will be slightly smaller than 1/2. To obtain agreement with the theoretical result, *A* should be 0.48. There are no experimental results for  $\langle\Delta\sigma\rangle_V$  in the vapor phase.

The shielding anisotropy in ice Ih has been measured by solid-state NMR with different multiple-pulse decoupling techniques to eliminate inhomogeneous dipolar broadening. Unfortunately, the results from the four reported studies do not converge. Two of the studies, using quite different decoupling methods, report  $\langle\Delta\sigma\rangle_V$  values of  $34 \pm 3$  ppm (at  $-90$  °C)<sup>54</sup> and  $34.2 \pm 1.0$  ppm (at  $-100$  °C).<sup>55</sup> We adopt the more precise of these results. The other two studies yield  $\langle\Delta\sigma\rangle_V \approx 28.5$  ppm (at  $-196$  °C).<sup>56</sup> The 5–6 ppm difference between these two sets of results cannot be attributed to the temperature; intramolecular vibrational averaging essentially involves only the vibrational ground state (see above) and the effect of intermolecular vibrational averaging can be estimated from the shielding surface<sup>25</sup> and thermal expansion coefficient of ice Ih to be about 0.1 ppm for a 100 K interval. Furthermore, averaging by rotational jumps only sets in at higher temperatures.<sup>80</sup> We favor the larger  $\langle\Delta\sigma\rangle_V$  value mainly because it agrees best with *ab initio* calculations. For a 17-molecule cluster with rigid ice Ih geometry, SCF calculations<sup>53</sup> with a large basis set yield  $\Delta\sigma = 34.8$  ppm. Using the calculated<sup>25</sup> bond-length dependence of the shielding anisotropy (inadvertently quoted in atomic units in ref 25),  $\partial\Delta\sigma/\partial r = -13.2$  ppm  $\text{\AA}^{-1}$ , this result can be corrected from  $r_{\text{OH}} = 1.01$   $\text{\AA}$ , as used in the calculation, to the experimentally derived<sup>81</sup> equilibrium bond length in ice Ih,  $r_{\text{OH}} = 0.973(5)$   $\text{\AA}$ . Making also a rovibrational correction of  $-1.08$  ppm (as for the monomer), we obtain  $\Delta\sigma = 34.2$  ppm. For a periodically replicated, static model of ice Ih (with  $r_{\text{OH}} = 0.993$   $\text{\AA}$ ), DFT calculations<sup>25</sup> yield  $\Delta\sigma = 33.5$  ppm and, after the same corrections, 32.7 ppm.

The experimental results for the isotropic shielding in ice Ih are more uncertain, mainly because they require large susceptibility corrections. One of the solid-state NMR studies<sup>56b</sup> was

**Table 1.** Proton Shielding Tensor in Different Phases of H<sub>2</sub>O<sup>a</sup>

phase	$\langle\sigma_{\text{iso}}\rangle_V$	$\langle\Delta\sigma\rangle_V$	$\langle\sigma_{\parallel}\rangle_V$	$\langle\sigma_{\perp}\rangle_V$
vapor	$30.2 \pm 0.1^{52}$	$19.1 \pm 0.1^{52}$	$42.9 \pm 0.1$	$23.8 \pm 0.1$
liquid at 80 °C	$26.22 \pm 0.02$	$25.1 \pm 0.4$	$43.0 \pm 0.3$	$17.9 \pm 0.1$
liquid at 27 °C	$25.71 \pm 0.02$	$27.4 \pm 0.1$	$44.0 \pm 0.1$	$16.6 \pm 0.1$
liquid at 0 °C	$25.41 \pm 0.02$	$28.5 \pm 0.2$	$44.4 \pm 0.1$	$15.9 \pm 0.1$
ice Ih	$21.1 \pm 0.5^{56b}$	$34.2 \pm 1.0^{55}$	$43.9 \pm 1.1$	$9.7 \pm 0.6$
vapor $\rightarrow$ Ice Ih	$-9.1 \pm 0.5$	$15.1 \pm 1.0$	$1.0 \pm 1.1$	$-14.1 \pm 0.6$
liquid, 80 $\rightarrow$ 0 °C	$-0.81 \pm 0.03$	$3.4 \pm 0.4$	$1.4 \pm 0.3$	$-2.0 \pm 0.1$

<sup>a</sup> Data for liquid water were obtained from eqs 26 and 27.

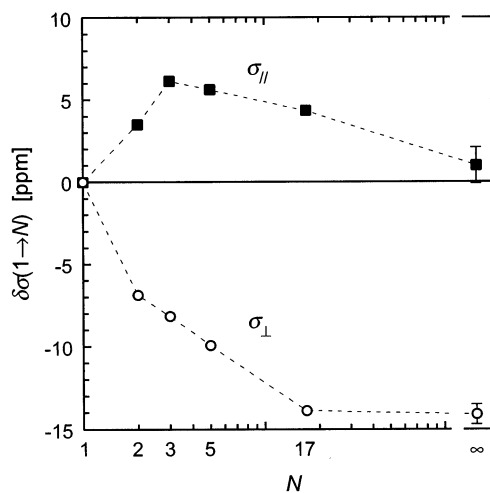


**Figure 7.** Association shift in the parallel and perpendicular proton shielding tensor components for progressive addition of water molecules to an ice Ih lattice, derived from *ab initio* SCF calculations with 4-31G (dimer–pentamer) or 6-311G(d,p) (17-mer) basis sets.<sup>53</sup> A correction for O–H bond lengthening in ice has been applied. The points with error bars represent the experimental vapor  $\rightarrow$  ice shift from Table 1.

carried out on a spherical single-crystal sample, for which the susceptibility contribution vanishes by symmetry. For this sample, a chemical shift of  $3.0 \pm 0.4$  ppm with respect to room-temperature water was reported.<sup>56b</sup> Assuming that the reference was a cylindrical sample ( $A = 1/2$ ) of water at 20 °C, we then obtain  $\langle\sigma_{\text{iso}}\rangle_V = 21.1 \pm 0.5$  ppm. This value, which we adopt, is not far from the (corrected) DFT result,<sup>25</sup>  $\langle\sigma_{\text{iso}}\rangle_V = 22.5$  ppm.

Table 1 summarizes what we consider to be the best available estimates of  $\langle\sigma_{\text{iso}}\rangle_V$  and  $\langle\Delta\sigma\rangle_V$  for the isolated water molecule and for water molecules in ice Ih. When these data are used to obtain the shielding tensor components parallel and perpendicular to the O–H bond, a striking feature is revealed: as a water molecule is transferred from the dilute vapor to the ice Ih lattice, there is a 60% deshielding perpendicular to the O–H bond but hardly any change in shielding along the bond ( $2 \pm 2\%$  increase). It would therefore seem that the perpendicular component  $\langle\sigma_{\perp}\rangle_V$  is much more sensitive to interaction effects. In contrast to these vapor  $\rightarrow$  ice shifts, the 80  $\rightarrow$  0 °C shifts in liquid water are of similar magnitude for  $\langle\sigma_{\parallel}\rangle_V$  and  $\langle\sigma_{\perp}\rangle_V$  (Table 1 and Figure 6). Because reduced temperature should enhance hydrogen bonding (making the liquid more icelike), one might expect to see the same qualitative trends in the two cases. Why is this not the case?

To resolve this apparent paradox, we make use of published *ab initio* results on the intermolecular perturbation of the water proton shielding tensor. Figure 7 shows the association shift  $\Delta\sigma(1 \rightarrow N) \equiv \sigma(N\text{-mer}) - \sigma(\text{monomer})$  for the two shielding components, calculated at the SCF level for clusters with rigid

(78) Raynes, W. T. In *Nuclear Magnetic Resonance: a Specialist Periodical Report*; The Chemical Society: London, 1978; Vol. 7, pp 1–25.

(79) Stratton, J. A. *Electromagnetic Theory*; McGraw-Hill: New York, 1941.

(80) Wittebort, R. J.; Usha, M. G.; Ruben, D. J.; Wemmer, D. E.; Pines, A. J. *Am. Chem. Soc.* **1988**, *110*, 5668–5671.

(81) Kuhs, W. F.; Lehmann, M. S. *Water Sci. Rev.* **1986**, *2*, 1–65.

icelike geometry ( $r_{\text{OH}} = 1.01 \text{ \AA}$ ,  $R_{\text{OO}} = 2.76 \text{ \AA}$ ).<sup>53</sup> We assume that the effect of rovibrational averaging cancels out in these differences. To allow comparison with the experimental vapor  $\rightarrow$  ice shift, we add a correction for the difference in equilibrium O–H bond length in vapor (0.958  $\text{\AA}$ )<sup>71,72</sup> and in ice Ih (0.973  $\text{\AA}$ ),<sup>81</sup> using  $\partial\sigma_{\parallel}/\partial r_{\text{OH}} = -80.4 \text{ ppm \AA}^{-1}$  and  $\partial\sigma_{\perp}/\partial r_{\text{OH}} = -19.8 \text{ ppm \AA}^{-1}$ .<sup>52,82</sup> It is evident from Figure 7 that, as the ice Ih lattice is progressively built up,  $\langle\sigma_{\perp}\rangle_{\text{V}}$  decreases monotonically whereas  $\langle\sigma_{\parallel}\rangle_{\text{V}}$  first increases at the dimer and trimer level but then decreases toward the ice Ih limit. Although most of these ab initio results were obtained with a rather small basis set (and without electron correlation), the calculations do seem to approach the experimental vapor  $\rightarrow$  ice shift. We conclude, therefore, that the small observed vapor  $\rightarrow$  ice shift in  $\langle\sigma_{\parallel}\rangle_{\text{V}}$  results from a partial cancellation of short-range and long-range intermolecular contributions.

In liquid water, the temperature shifts in  $\langle\sigma_{\parallel}\rangle_{\text{V}}$  and  $\langle\sigma_{\perp}\rangle_{\text{V}}$  are in the same direction as the theoretical dimer shifts. SCF calculations with an extended basis set (close to the Hartree–Fock limit for the shielding) yield  $\delta\sigma_{\parallel}(1\rightarrow 2) = +4.2 \text{ ppm}$  and  $\delta\sigma_{\perp}(1\rightarrow 2) = -5.8 \text{ ppm}$  for  $r_{\text{OH}} = 0.957 \text{ \AA}$  and  $R_{\text{OO}} = 2.976 \text{ \AA}$ .<sup>83</sup> The experimental 80  $\rightarrow$  0  $^{\circ}\text{C}$  shifts in liquid water (Table 1) are precisely one-third of these dimer shifts. The fact that the individual components of the shielding tensor are affected in the same way by decreasing temperature in the liquid as by partial (33%) dimerization in the vapor indicates that the shielding tensor reports mainly on local changes in the liquid structure. This can be reconciled with the ice Ih results if the long-range contribution to  $\langle\sigma_{\parallel}\rangle_{\text{V}}$ , responsible for the nonmonotonic behavior of the association shift (Figure 7), is essentially independent of temperature.

Most previous attempts at extracting information about the structure of liquid water from the observed temperature dependence of  $\langle\sigma_{\text{iso}}\rangle_{\text{V}}$  have postulated a two-state model, where an OH group in a water molecule can exist in either of two discrete states: hydrogen bonded (HB) or free (F). Assuming that the observed shielding tensor is averaged over these two states, we can write for its two components

$$\langle\sigma_{\parallel}\rangle_{\text{V}} = f(T)\sigma_{\parallel}^{\text{F}} + [1 - f(T)]\sigma_{\parallel}^{\text{HB}} \quad (28\text{a})$$

$$\langle\sigma_{\perp}\rangle_{\text{V}} = f(T)\sigma_{\perp}^{\text{F}} + [1 - f(T)]\sigma_{\perp}^{\text{HB}} \quad (28\text{b})$$

where  $f(T)$  is the fraction of free (not hydrogen-bonded) OH

(82) Augspurger, J. D.; Dykstra, C. E. *Mol. Phys.* **1993**, *80*, 117–126.

(83) Chestnut, D. B.; Rusiloski, B. E. *J. Phys. Chem.* **1993**, *97*, 2839–2845.

groups at temperature  $T$ . Taking the temperature derivative of eq 28 and equating  $\sigma_{\perp}^{\text{HB}} - \sigma_{\perp}^{\text{F}}$  with the vapor dimerization shift  $\delta\sigma_{\parallel}(1\rightarrow 2)$ , we obtain  $df/dT = -(d\langle\sigma_{\parallel}\rangle_{\text{V}}/dT)/\delta\sigma_{\parallel}(1\rightarrow 2)$  and similarly for the perpendicular component. Inserting the experimental temperature derivatives (Figure 6) and the theoretical dimerization shifts<sup>83</sup> in these two relations, we obtain, as required by the model, the same value for  $df/dT$ . However, this value,  $df/dT = 0.0043 \text{ K}^{-1}$ , implies that 35% of all OH groups go from the hydrogen bonded to the free state as the temperature is raised from 0 to 80  $^{\circ}\text{C}$ . This result cannot be reconciled, for any reasonable hydrogen-bond definition, with the nearly temperature independent tetrahedral coordination in liquid water seen in molecular dynamics simulations<sup>84</sup> and implied by X-ray and neutron diffraction data.<sup>85,86</sup> Moreover, with such a large variation in  $f$  over an 80  $^{\circ}\text{C}$  interval, it would be hard to explain the continuous variation of the (isotropic) shielding that has been observed all the way from deeply supercooled water (down to  $-90 \text{ }^{\circ}\text{C}$ )<sup>87</sup> to the supercritical fluid (up to 400  $^{\circ}\text{C}$ ).<sup>88,89</sup> Finally, the high-frequency shoulder of the O–H stretching band in the Raman spectra, which has been linked to free OH groups, indicates that  $f$  is doubled from 0 to 100  $^{\circ}\text{C}$ .<sup>90</sup> But if  $f$  increases linearly with temperature with a slope  $df/dT = 0.0043 \text{ K}^{-1}$ , as implied by the two-state interpretation of our shielding data, then a doubling of  $f$  from 0 to 100  $^{\circ}\text{C}$  requires that  $f = 0.43$  at 0  $^{\circ}\text{C}$  and  $f = 0.86$  at 100  $^{\circ}\text{C}$ . This is 2 orders of magnitude more than the Raman estimate of  $f = 0.01\text{--}0.02$  at room temperature.<sup>90</sup> In summary, we believe that a two-state model is far too crude to capture the subtle variations in the structure of liquid water structure that occur in the 0–100  $^{\circ}\text{C}$  range. Clearly, a more detailed analysis is needed that quantitatively takes into account the dependence of the shielding tensor components on the hydrogen-bond length and angle.<sup>33</sup>

**Acknowledgment.** We thank Dr. Bernd Pfrommer for providing results of DFT calculations of the full shielding tensor in liquid water and Charlotta Damberg for assistance with the 800 MHz spectrometer at the Swedish NMR Center. This work was supported by the Swedish Research Council.

JA026981S

(84) Svishev, I. M.; Kusalik, P. G. *J. Chem. Phys.* **1993**, *99*, 3049–3058.

(85) Narten, A. H.; Levy, H. A. *J. Chem. Phys.* **1971**, *55*, 2263–2269.

(86) Bosio, L.; Chen, S.-H.; Teixeira, J. *Phys. Rev. A* **1983**, *27*, 1468–1475.

(87) Chen, L.; Gross, T.; Lüdemann, H.-D. *Z. Naturforsch.* **2000**, *55a*, 473–477.

(88) Hoffmann, M. H.; Conradi, M. S. *J. Am. Chem. Soc.* **1997**, *119*, 3811–3817.

(89) Matubayasi, N.; Wakai, C.; Nakahara, M. *J. Chem. Phys.* **1997**, *107*, 9133–9140.

(90) Giguère, P. A.; Pigeon-Gosselin, M. *J. Raman Spectrosc.* **1986**, *17*, 341–344.